Control of Camless Intake Process (Part II)

M.-S. S. Ashhab, A. G. Stefanopoulou*
Mechanical and Environmental Engr. Dept.
University of California, Santa Barbara

J. A. Cook, M. B. Levin
Ford Motor Company
Scientific Research Laboratory, Dearborn

Abstract

A model-based control scheme is designed to regulate the cylinder air charge of a camless multicylinder engine for unthrottled operation. The controller consists of a feedforward and an adaptive feedback scheme based on a control-oriented model of the breathing process of an engine equipped with electro-hydraulic springless valve-train. The nonlinear control scheme is designed to achieve cylinder-to-cylinder balancing, fast cycle-to-cycle response, and minimization of pumping losses. The algorithm uses conventional sensor measurements of intake manifold pressure and mass air flow to the intake manifold, and intake valve duration measurement. Closed loop simulation results are shown for a four cylinder engine.

1 Introduction

In this paper we develop an adaptive controller for a camless engine equipped with electro-hydraulic springless valvetrain. The scheme amounts to control electronically the air flow into each cylinder using individual intake valve actuation. This results in decoupling the driver from the engine and allows better optimization over a wide operating range based on pedal position and estimated torque demand. Pumping losses are significantly reduced because conventional engine throttling is eliminated and replaced by early valve closing or valve lift control whenever necessary. Eliminating the slow intake manifold filling dynamics leads to faster breathing characteristics and can potentially increase the transient torque performance.

The major challenge in camless operation of a spark ignition engine is controlling the cylinder air charge rapidly and accurately based on conventional measurements. The feedback controller has to ensure regulation of the air charge trapped in the cylinders in order to be seamlessly integrated with the air-to-fuel ratio and spark timing control algorithms of a conventional engine management system. Specifically, the difficulty in controlling camless cylinder air charge arises from the following issues: Firstly, the controller has to correctly balance cylinder-to-cylinder variations and, at the same time, provide correction for slowly varying parameters in the engine and valve-train components. Secondly, cylinder-to-cylinder control must be achieved using conventional engine sensors such as temperature, pressure, and flow into the intake manifold.

The developed controller addresses these two issues. It employs an adaptive feedforward scheme that regulates individual intake valve lift (IVL) and intake valve duration (IVD) based on mass air flow and intake manifold pressure measurements. The feedforward controller ensures fast tracking response of the cylinder air charge demand. The desired cylinder air charge (m^{des}) that the variable valve controller must track can be specified by a nonlinear function of the pedal position and engine speed as shown in Figure 1. As Figure 1 shows, the controller consists of (i) a feedforward controller C, (ii) cylinder air charge estimator, and (iii) on-line parameter estimator. The adaptation enables robust cylinder-to-cylinder and cycle-to-cycle operation; it is based on the individual cylinder air charge estimation using existing intake manifold measurements. Furthermore, the controller minimizes pumping losses by choosing an appropriate combination of IVL and IVD.

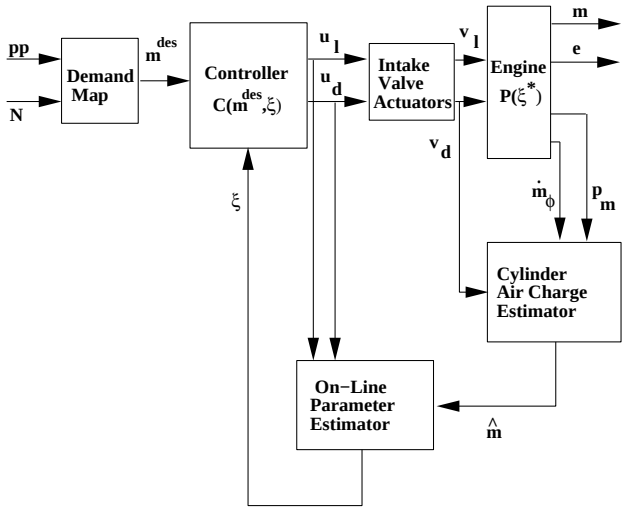

Figure 1: Block diagram of the adaptive feedforward control scheme.

The paper is organized as follows. In Section 2 we derive the optimum steady-state values for lift and duration that minimize pumping losses. The feedforward controller, C, uses the desired cylinder air charge, m^{des}, to calculate the control signals, u_l and u_d to the actuators

* Corresponding author, e-mail: anna@engineering.ucsb.edu, phone: 805/893-8501, fax: 805/893-8651. Research supported in part by the National Science Foundation under contract NSF ECS-97-33293 and the Department of Energy Cooperative Agreement No. DE-FC02-98EE50540; matching funds were provided by FORD MO. CO.

as described in Section 3. The electro-hydraulic actuators provide to the engine an intake valve lift v_l and duration v_d, which in general, are different from the control command $(u_l,\, u_d)$. The controller objective is to ensure that the real engine cylinder air charge is equal to the desired cylinder air charge, while minimizing the pumping loss. The available measurements from the engine are the manifold pressure, p_m, the mass air flow through the throttle, $\dot{m}_\phi$, and the actual intake valve duration, v_d. These three measurements are used to get an estimate of the cylinder air charge, $\hat{m}$, as described in subsection 4. The on-line parameter estimator uses the estimated cylinder air charge, $\hat{m}$, to adapt the controller parameters, ξ.

2 Optimization

The feedforward controller is based on the mean-value cylinder breathing characteristics developed in Part I. It calculates the control signals, namely, intake valve lift, u_l, and duration, u_d, to satisfy the cylinder air charge demand, m^{des}, and to minimize the specific pumping losses, e. The desired cylinder air charge (m^{des}) that the engine controller must track can be specified by a nonlinear function of the pedal position and engine speed as shown in Figure 1. This function is usually called *"Demand Map"* and is developed by experienced drivers and calibrators.

In Part I, it is shown that the cylinder air charge (m), and the corresponding specific pumping losses (e) at constant engine speed can be expressed as

$$\begin{aligned} m(t+\Delta T) &= F_m(u_l(t), u_d(t)) \\ e(t+\Delta T) &= F_e(u_l(t), u_d(t)), \end{aligned} \tag{1}$$

using the nominal cylinder air charge, F_m^o, and specific pumping loss, F_e^o, at the specific engine speed. Using the F_m surface we find the set, S_m, of lift and duration commands that satisfies the cylinder air charge demand, m^{des}, as shown in (Ashhab et al., 1998):

$$S_m = [u_l^m, u_d^m] \text{ such that } F_m(u_l^m, u_d^m) = m^{des}. \tag{2}$$

To illustrate the above mechanism, consider the intersection of the m^{des} plane with the F_m surface as shown in Figure 2. The curve in the u_l and u_d plane in Figure 2 shows the selected u_l^m and u_d^m in response to a command $m^{des} = 0.3$ g per intake event. The curve marked by ("o") in Figure 3 shows the projection of S_m on the F_e surface and indicates the corresponding pumping losses. It is evident that as u_d^m decreases in S_m – u_l^m has to increase to maintain constant cylinder air charge – the pumping loss decreases. Therefore, the pair $u = (u_l^m, u_d^m)$ that satisfies m^{des} and minimizes the pumping loss approaches $(\infty, 0)$ which is obviously infeasible to attain and unrealistic to ask.

There are two considerations that when taken into account prevent u_l^m from being very large and u_d^m from being very small. Firstly, sensitivity analysis of the performance variables to the intake valve lift performed in (Ashhab et al., 1998) and observation of the surfaces F_m and F_e in Figures 2 and 3 show that cylinder air charge and pumping loss are insensitive to changes in the lift for large values of lift. In Part I, we baptized this effect as "lift saturation." It denotes the reduced actuator authority for large values of lift. From a control design perspective there is no benefit from increasing u_l^m beyond this saturation value, $u_{l_{sat}}$, even if it is feasible from physical considerations. The value of $u_{l_{sat}}$ depends on engine speed (N), namely, $u_{l_{sat}}$ is an increasing function of speed. For simplicity, we assume that $u_{l_{sat}}$ is constant for all engine speeds. This introduces an upper bound for the lift command

$$u_l^m \le u_{l_{sat}}. \tag{3}$$

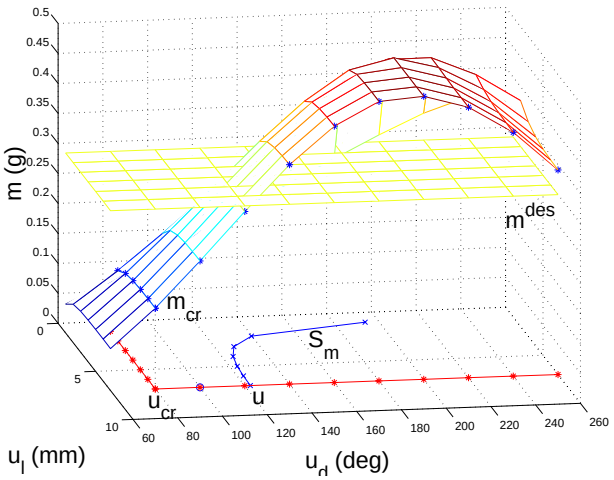

Figure 2: Cylinder air charge requirements and optimality constraints for operation at 1500 rpm.

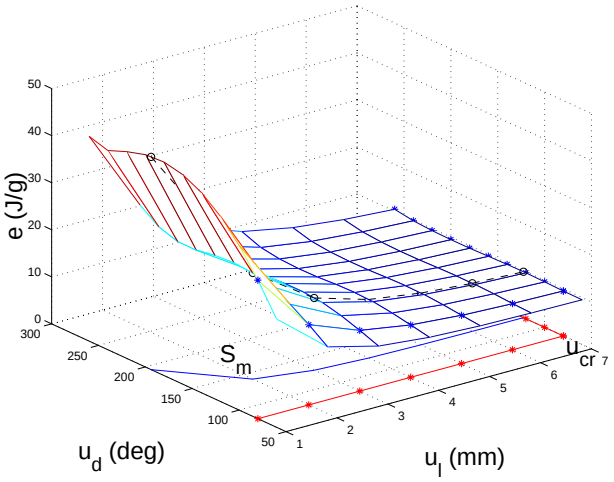

Figure 3: Pumping loss minimization at 1500 rpm.

Recall here that the electro-hydraulic energy required by the springless actuator increases with valve lift, which

is a fact that reinforces our strategy for not requiring large lift commands. A suitable value for $u_{l_{sat}}$ for the engine specifications in this work is 7 mm.

Secondly, analytical and experimental work in (Urata et al., 1993; Voget et al., 1996) show that engine operation with early valve closing is often coupled with combustion problems because small valve duration inhibits mixing and reduces significantly the mixture temperature during expansion. In addition, there is a severe tradeoff between small valve duration and quiet seating (Schechter and Levin, 1996). To maintain stable combustion and low noise levels we introduce a lower bound for the duration command

$$u_d^m \geq u_{d_{sat}}. \tag{4}$$

A reasonable value for the minimum valve duration is assumed to be $u_{d_{sat}} = 80^o$.

The constraints (3) and (4) are shown by the "**L**" shape marked by "*" in the (u_l, u_d) plane in Figures 2 and 3. We define the cylinder air charge at $(u_{l_{sat}}, u_{d_{sat}})$ as the critical cylinder air charge, $m_{cr} = F_m(u_{l_{sat}}, u_{d_{sat}})$. Note that if $m^{des} \leq m_{cr}$ then the pair (u_l, u_d) that minimizes the pumping loss under the constraints (3) and (4) is $(u_l, u_{d_{sat}})$ with $u_l \leq u_{l_{sat}}$. On the other hand, if $m^{des} \geq m_{cr}$ then the pair (u_l, u_d) that minimizes the pumping loss is $(u_{l_{sat}}, u_d)$ with $u_d \geq u_{d_{sat}}$. In Figure 2, $m^{des} = 0.3$ g is larger than $m_{cr} = 0.24$ g. The intersection of S_m with the given constraints provides the pair $u = (7\text{mm}, 122^o)$ that results in the minimum pumping loss.

3 Adaptive Feedforward Controller

The feedforward controller selects the pair $u = (u_l, u_d)$ that satisfies the desired cylinder air charge m^{des} and belongs to the "**L**" shaped set. A look-up table using data from the nominal simulation engine model or experimental data can be used to realize the feedforward scheme described above. The drawback associated with this approach stems from the need to adapt the feedforward controller in order to count for engine parameter variations and uncertainty. To this end, we parameterize the cylinder air charge data using a finite basis function $\beta_i, i = 1, \ldots, m$. With slight abuse of notation and for simplicity, we use two arguments for the real breathing characterization, $m = F_m(u_l, u_d)$, and three arguments for its finite basis approximation, $m \approx F_m(u_l, u_d, \xi)$:

$$\begin{aligned} &F_m(u_l, u_d, \xi) = \beta^T(u_l, u_d)\xi = \\ &\beta_1(u_l, u_d)\xi_1 + \beta_2(u_l, u_d)\xi_2 + \cdots + \beta_m(u_l, u_d)\xi_m. \end{aligned} \tag{5}$$

The known functions $\beta_i, i = 1, \ldots, m$, of u_l and u_d are called the regression variables. The vector parameter ξ is determined such that the difference between the cylinder air charge computed using equation (5) and the real cylinder air charge is minimum in the least squares sense. We initialize the parameter $\xi = \xi^o$ based on the nominal cylinder air charge at 1500 RPM, F_m^o, such that:

$$\begin{aligned} &F_m^o(u_l, u_d) \approx F_m(u_l, u_d, \xi^o) = \beta^T(u_l, u_d)\xi^o \\ &= \beta_1(u_l, u_d)\xi_1^o + \beta_2(u_l, u_d)\xi_2^o + \cdots + \beta_m(u_l, u_d)\xi_m^o. \end{aligned} \tag{6}$$

Real-time estimation of ξ based on engine measurements enables adaptation of the function $F_m(u_l, u_d, \xi)$. This will be discussed in the On-Line Parameter Estimation section. Because of the finite dimension of our basis function, the adaptation algorithm cannot in general guarantee convergence to the real cylinder breathing characteristics ($m = F_m(u_l, u_d, \xi)$).

Based on the estimated parameter ξ we define the cylinder air charge that corresponds to the upper bound of lift and the lower bound of duration as $g_d(u_d)$ and $g_l(u_l)$, equivalently:

$$g_d(u_d) := F_m(u_{l_{sat}}, u_d, \xi) \text{ and } g_l(u_l) := F_m(u_l, u_{d_{sat}}, \xi). \tag{7}$$

The feedforward controller can be written as

$$\begin{aligned} &C(m^{des}, \xi) = \\ &(u_l, u_d) = \begin{cases} (u_{l_{sat}}, g_d^{-1}(m^{des})) & \text{if} \quad m^{des} \geq m_{cr} \\ (g_l^{-1}(m^{des}), u_{d_{sat}}) & \text{if} \quad m^{des} \leq m_{cr} \end{cases}' \end{aligned} \tag{8}$$

where, the inverse functions g_d^{-1} and g_l^{-1} are implemented using nonlinear root finding techniques.

3.1 On-line Parameter Estimation

The feedforward controller is a linear function of the parameter ξ which can be estimated on-line assuming cylinder air charge measurements ($\hat{m}$). The estimation is needed in adjusting the feedforward controller to compensate for variations in the individual camless valvetrain actuators and engine component characteristics. Sources of parameter variations can be summarized as follows.

- The characteristics (slopes, closing, opening, and seating) of the electro-hydraulic springless actuators depend on component size variations, oil viscosity, temperature and oil-air contents.
- The intake valve effective area (A_v) depends on deposits and wear.
- The geometric parameters of the engine tend to be uncertain due to manufacturing errors and tolerances.
- Variations in temperature and engine speed affect the cylinder breathing characteristics. The feedforward controller has been developed for constant temperature and engine speed.
- Flow restrictions and vehicle body geometry impose parametric uncertainty to the air flow through the throttle body.

In addition to the parametric uncertainty the mean-value model characterization of the multicylinder breathing process introduces several sources of unstructured uncertainty:

- high order actuator dynamics (see Part I)
- sensor dynamics
- Helmholtz dynamics (see Part I)

Based on the calculated cylinder air charge ($\hat{m}$) the on-line parameter estimator uses the recursive least-squares algorithm to update the feedforward controller parameter ξ. We update ξ at time step j using the information at time step $j-1$, and the observed cylinder air charge and inputs at time step j, $\hat{m}(j)$ and $u(j)$. Namely, the parameter ξ is adjusted so that $\hat{m}$ is approximated as well as possible in the finite dimensional space defined by the basis functions $\beta = [\beta_1, \ldots, \beta_m]$. It can be shown that ξ should be updated in the subspace defined by the basis functions $\beta(j) = \beta(u(j))$:

$$\xi(j) = \xi(j-1) + \alpha\beta(j). \tag{9}$$

The following fact is used to evaluate α : $\hat{m}(j) = \beta(j)^T\xi(j) = \beta(j)^T\xi(j-1) + \alpha\beta(j)^T\beta(j)$. Solving for α, we get $\alpha = \frac{1}{\beta(j)^T\beta(j)}\left(\hat{m}(j) - \beta(j)^T\xi(j-1)\right)$. Therefore, equation (9) reduces to the Kaczmarz's algorithm (Astrom and Wittenmark, 1989):

$$\xi(j) = K(u(j), \hat{m}(j), \xi(j-1)) =$$

$$\xi(j-1) + \frac{\beta(j)}{\beta(j)^T\beta(j)}\left(\hat{m}(j) - \beta(j)^T\xi(j-1)\right). \tag{10}$$

The algorithm is initialized at $j = 1$ with $\xi(j-1) = \xi^o$ and performed for each cylinder separately. Recall, ξ^0 is the feedforward controller parameter obtained from nominal engine data. In case of excess noise or random error in the estimated cylinder cylinder air charge $\hat{m}$, the updating formula for the parameter ξ is modified to the stochastic approximation algorithm:

$$\xi(j) = \xi(j-1) + P(j)\beta(j)\left(\hat{m}(j) - \beta(j)^T\xi(j-1)\right), \tag{11}$$

where, $P(j) = \left(\sum_{k=1}^{j}\beta(k)\beta(k)^T\right)^{-1}$.

4 Cylinder Air Charge Estimation

The controller designed thus far is based on accurate estimation of the individual cylinder air charge to update the feedforward controller parameters. It is important, therefore, to derive a cylinder air charge estimator based on conventional and inexpensive sensors. In this section we describe how to use the mass air flow through the throttle body (MAF) and intake manifold absolute pressure (MAP) measurements to extract information about the actual air trapped in each individual cylinder.

We start by summarizing the state-space representation of the multicylinder breathing dynamics. Let the state vector $\chi = \left[\begin{array}{cccc} p_m & p_{c_1} & \ldots & p_{c_n}\end{array}\right]^T$, then,

$$\begin{aligned}
\dot{\chi} &= f\left(\chi, \left[\begin{array}{c} u_{l_1} \\ \vdots \\ u_{l_n}\end{array}\right], \left[\begin{array}{c} u_{d_1} \\ \vdots \\ u_{d_n}\end{array}\right]\right), \\
\left[\begin{array}{c} m_{c_1} \\ \vdots \\ m_{c_n}\end{array}\right] &= h_z(\chi), \text{ performance variables} \\
\left[\begin{array}{c} p_m \\ m_\phi\end{array}\right] &= h_y(\chi), \text{ measurements,}
\end{aligned}$$

where, p_m is the intake manifold pressure, p_{c_i} is the ith cylinder pressure, m_{c_i} the ith cylinder air charge, and u_{l_i} and u_{d_i} the valve lift and duration respectively.

By processing the measured outputs using MAP and MAF sensors we calculate the quantities:

$$y_k = -\frac{V_m}{RT}(p_m((k+1)\Delta) - p_m(k\Delta)) + \int_{k\Delta}^{(k+1)\Delta}\dot{m}_\phi(t)dt, \tag{12}$$

which we call induced measurements. Intake manifold pressure is sampled at least every fundamental event ($\Delta = \frac{120}{nN}$) triggered by crankangle position when each cylinder reaches top dead center (TDC). Mass air flow is measured and averaged over each fundamental event. Figure 4 shows schematically the signal processing for the induced measurements. The inputs to the engine, u_{l_k} and u_{d_k}, are applied at time $k\Delta$ (beginning of event k), while the quantity y_k is obtained at time $(k+1)\Delta$ (end of event k). Thus, y_k is delayed by a fundamental event from the inputs to the engine. Let the state-to-induced measurements map be

$$y_k = F_y\left(\chi_{[k\Delta,(k+1)\Delta]}\right). \tag{13}$$

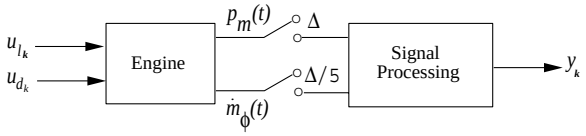

Figure 4: Signal processing for the induced measurements.

The induced measurements contain information for the individual cylinder air charge. Recall the equation governing the rate of change of manifold pressure:

$$\frac{dp_m(t)}{dt} = \frac{RT}{V_m}\left[\dot{m}_\phi(t) - \sum_{i=1}^{n}\dot{m}_{c_i}(t)\right]. \tag{14}$$

Integration of equation (14) over a fundamental event results in

$$p_m((k+1)\Delta) - p_m(k\Delta) =$$

$$\frac{RT}{V_m}\left[\int_{k\Delta}^{(k+1)\Delta}\dot{m}_\phi(t)dt - \int_{k\Delta}^{(k+1)\Delta}\sum_{i=k-n+1}^{k}\dot{m}_{c_i}(t)dt\right].$$

Rearranging this equation and using (12) leads to

$$y_k = \int_{k\Delta}^{(k+1)\Delta} \sum_{i=k-n+1}^{k} \dot{m}_{c_i}(t)dt. \qquad (15)$$

First, note that in the case of a 4-cylinder engine with $IVD_i < 180^o$ $i = 1,\ldots,4$ each cylinder has separate breathing process from all the other cylinders (no cylinder overlap), and the induced measurement y_k at time $(k+1)\Delta$ corresponds to the cylinder air charge of cylinder k

$$y_k = \int_{k\Delta}^{(k+1)\Delta} \dot{m}_{c_k}(t)dt = m_{c_k}. \qquad (16)$$

Secondly, consider the breathing conditions during the event $[k\Delta,(k+1)\Delta]$ with r cylinders simultaneously interacting with the intake manifold, i.e., with r-cylinder overlap. The quantity y_k can be expressed in terms of the cylinder air charge of cylinders $k-r+1,\ldots,k$:

$$y_k = \int_{k\Delta}^{(k+1)\Delta} \sum_{i=k-n+1}^{k} \dot{m}_{c_i}(t)dt =$$

$$\int_{k\Delta}^{(k+1)\Delta} \dot{m}_{c_{k-r+1}}(t)dt + \cdots + \int_{k\Delta}^{(k+1)\Delta} \dot{m}_{c_k}(t)dt. \qquad (17)$$

Let the fraction of the ith cylinder air charge during event k be (see Figure 5)

$$\mu_k^i = \frac{1}{m_i} \int_{k\Delta}^{(k+1)\Delta} \dot{m}_{c_i}(t)dt. \qquad (18)$$

The induced measurement (Eq. 15) can now be expressed as

$$y_k = \mu_k^{k-r+1} m_{k-r+1} + \cdots + \mu_k^k m_k, \qquad (19)$$

where, m_i, $i = k-r+1,\ldots,k$ is the cylinder air charge of cylinder i. It is evident that $\sum_{k=l}^{l+r-1} \mu_k^l = 1$. The fraction μ_k^i depends on the valve lift and duration of cylinder i and can be pre-calculated based on nominal engine data. It is obvious that in case of unknown cylinder-to-cylinder maldistribution the nominal μ_k^i will differ from the real fractions, μ_k^i. By construction, however, the error in the fractions μ's will be smaller than the error in the cylinder air charge.

To simplify the discussion we first consider the case of the 4-cylinder engine. The intake valve duration (u_d) is normally less than 360^o. Thus, even during malfunction in the actuator closing timing, we can safely assume that there is at most 2-cylinder overlap ($r = 2$). We then provide the general procedure for the cylinder air charge estimation for arbitrary number of cylinders (n) and arbitrary number of cylinder overlap (r).

4.1 4-cylinder Engine Case

At low-to-medium engine speeds there is no need for cylinder overlap for the 4-cylinder 4-stroke engine. For high speeds, however, operating with $IVD > 180^o$ is required in order to achieve maximum torque. Recall from Part I, that at high speed there is not enough time for the intake valve to reach maximum lift, thus, it is necessary to increase the duration beyond bottom dead center (BDC). Specifically, there is a 2-cylinder overlap ($r = 2$) in the 4-cylinder engine at an engine speed of 6000 RPM with an intake valve duration equal to 260^o. Recall that the event duration is 180^o of crank angle. Using the measurements during cycle j and equation (19), we calculate the following induced measurements:

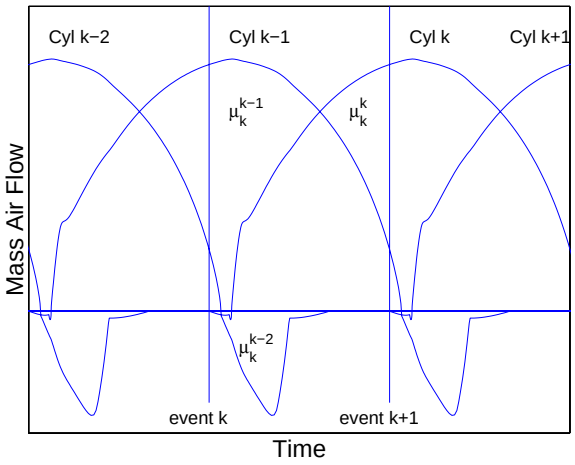

Figure 5: Mass air flow and air mass fractions of 3-cylinder overlap.

$$\begin{aligned} y_{4j} &= \mu_{4j}^{4j-1} m_{4j-1} + \mu_{4j}^{4j} m_{4j} \\ y_{4j+1} &= \mu_{4j+1}^{4j} m_{4j} + \mu_{4j+1}^{4j+1} m_{4j+1} \\ y_{4j+2} &= \mu_{4j+2}^{4j+1} m_{4j+1} + \mu_{4j+2}^{4j+2} m_{4j+2} \\ y_{4j+3} &= \mu_{4j+3}^{4j+2} m_{4j+2} + \mu_{4j+3}^{4j+3} m_{4j+3}. \end{aligned} \qquad (20)$$

For constant valve inputs the engine reaches its equilibrium which is a limit cycle, and consequently each of the arguments in Eq. 20 becomes periodic (with period 4). This inherent periodic nature of the breathing process allows us to lift the linear time-variant (LTV) system to a 4-input 4-output linear time invariant (LTI) system:

$Y_j = A_j M_j$ or, in expanded form,

$$\begin{bmatrix} y_{4j} & y_{4j+1} & y_{4j+2} & y_{4j+3} \end{bmatrix}^T =$$

$$\begin{bmatrix} 1-\mu_{4j-1}^{4j-1} & \mu_{4j}^{4j} & 0 & 0 \\ 0 & 1-\mu_{4j}^{4j} & \mu_{4j+1}^{4j+1} & 0 \\ 0 & 0 & 1-\mu_{4j+1}^{4j+1} & \mu_{4j+2}^{4j+2} \\ \mu_{4j-1}^{4j-1} & 0 & 0 & 1-\mu_{4j+2}^{4j+2} \end{bmatrix} \times$$

$$\begin{bmatrix} m_{4j-1} & m_{4j} & m_{4j+1} & m_{4j+2} \end{bmatrix}^T,$$

where, we exploit the fact that $m_{4j+3} = m_{4j-1}$, $\mu_{4j+3}^{4j+3} = \mu_{4j-1}^{4j-1}$, and $\mu_k^{k-1} = 1-\mu_{k-1}^{k-1}$, for all k during quasi-static

engine conditions. Note that Y_j is the measurement vector and M_j is the cylinder air charge vector. To ensure that the periodic conditions are satisfied we perform the estimation only during constant pedal position which does not require changes in valve inputs. Note also that the cylinder air charge vector lags the measurement vector by $(r-1)$ events, where r is the maximum number of cylinders drawing air from the intake manifold ($r = 2$ in 4-cylinder case). Estimation of the cylinder air charge vector depends on the values of the entries of matrix A_j, i.e., the values of the mass fractions (μ_k^k). Values for the μ_k^k are calculated using the nominal simulation model. Figures 6 and 7 show nominal μ_k^k data as functions of v_d and v_l at engine speeds of 1500 and 6000 RPM, respectively. For the estimator implementation we ignore the small dependence of μ_k^k on v_l.

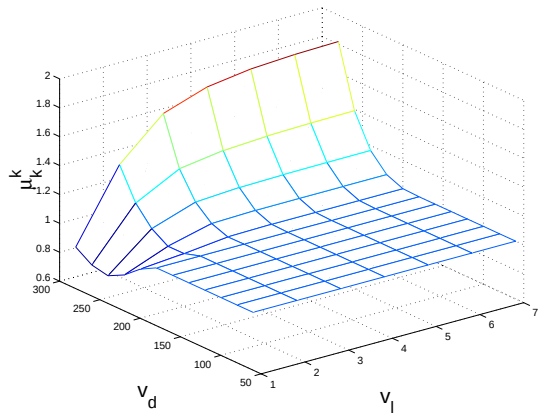

Figure 6: Nominal μ_k^k as a function of v_d for a 4-cylinder engine at an engine speed of 1500 RPM.

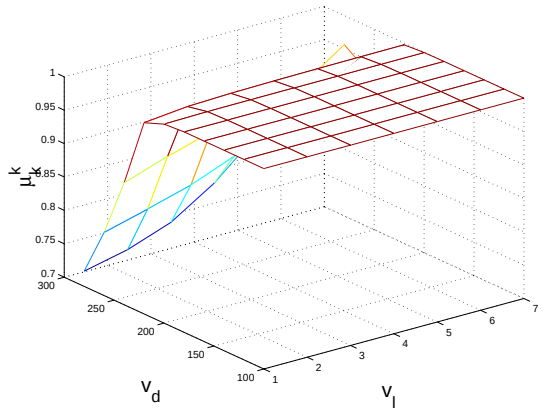

Figure 7: Nominal μ_k^k as a function of v_d for a 4-cylinder engine at an engine speed of 6000 RPM.

A qualitative description of the nonlinear behavior of the μ_k^k's follows. Note that if $v_d < 180^o$ then $\mu_k^k = 1$ since there is no cylinder overlap ($r = 1$). For $v_d > 180^o$, two distinct patterns of behavior are observed. First, consider the case where the mass air flow into the cylinder ($\dot{m}_c$) is positive until the intake valve closes. The fraction of the cylinder air charge during the first 180^o (μ_k^k) will be less than 1. Indeed, this happens at $N = 1500$ RPM and small intake valve lifts, (v_l), and at $N = 6000$ RPM for the whole range of lifts (v_l=1-7 mm). A completely different behavior for the μ_k^k is observed when the air flow into the cylinder reverses its direction at some value $v_d = v_{d_o} > 180^o$. In this case, the fraction μ_k^k is a decreasing function of v_d in the range $180^o < v_d < v_{d_o}$, and increases with v_d for $v_d > v_{d_o}$ (according to Eq. (18)). In Figure 6 the value of μ_k^k is greater than 1 for $v_d > 180^o$ and $v_l > 3$ mm due to the backward air flow from the cylinder into the runners after bottom dead center.

Observability of the individual cylinder air charge depends on the the values of μ_k^k. Namely, the determinant of the matrix A_j is calculated as

$$\det(A_j) = (1-\mu_{4j-1}^{4j-1})(1-\mu_{4j}^{4j})(1-\mu_{4j+1}^{4j+1})(1-\mu_{4j+2}^{4j+2}) - \mu_{4j-1}^{4j-1}\mu_{4j}^{4j}\mu_{4j+1}^{4j+1}\mu_{4j+2}^{4j+2} \quad (21)$$

is always nonzero because $\mu_l^l > 0.5$ for $l = 4j-1, 4j, 4j+1, 4j+2$. The estimated cylinder air charge can be found by $M_j = A_j^{-1} Y_j$.

4.2 General Case

Individual cylinder air charge estimation for arbitrary number of cylinders, n, and arbitrary (but reasonable $r \leq \frac{n}{2}$) number of cylinder overlap, r, is given by

$$\begin{bmatrix} y_{nj} & y_{nj+1} & \dots & y_{nj+n-1} \end{bmatrix}^T = \begin{bmatrix} \mu_{nj}^{nj-(r-1)} & \mu_{nj}^{nj-(r-1)+1} & \dots & 0 \\ 0 & \mu_{nj+1}^{nj-(r-1)+1} & \dots & 0 \\ \vdots & \vdots & \vdots & \vdots \\ \mu_{nj-1}^{nj-(r-1)} & \mu_{nj-1}^{nj-(r-1)+1} & \dots & \mu_{nj+n-1}^{nj-(r-1)+n-1} \end{bmatrix} \times \begin{bmatrix} m_{nj-(r-1)} & m_{nj-(r-1)+1} & \dots & m_{nj-(r-1)+(n-1)} \end{bmatrix}^T \quad (22)$$

As in the 4-cylinder engine case, the observability of the individual cylinder air charge depends on the determinant of the $n \times n$ matrix in (22), and consequently, on the values of μ_k^k. The following lift and duration values result in conditions for an unobservable system:

8-cylinder engine	12-cylinder engine
$v_l = 4$mm and $v_d = 178.1^o$	$v_l = 4$mm and $v_d = 102.7^o$
$v_l = 3$mm and $v_d = 174.4^o$	$v_l = 8$mm and $v_d = 104.3^o$

The above lift and duration values are few examples for which the $n \times n$ matrix ($n = 8$ or $n = 12$) in (22) becomes singular. During operation under unobservable conditions the estimation algorithm can be deactivated. For other conditions where this matrix is not singular the estimated cylinder air charge can be found by using (22).

5 Closed Loop Controller Algorithm

In this section we describe the closed loop algorithm merging the adaptive feedforward controller (Section 3) with the cylinder air charge estimation (Section 4). It is important to note here that cylinder air charge estimation and the windowing process is reset when there is a change in cylinder air charge demand (m^{des}) or engine speed (N). The resetting mechanism can be implemented using a bound that depends on the signal-to-noise ratio of the pedal position and speed sensor.

In the following two subsections we discuss the iterative closed loop agorithm for the 4-cylinder engine in detail, and we formulate the general algorithm for an n-cylinder engine with r-cylinder overlap.

5.1 4-Cylinder Engine Case

With no loss of generality, the algorithm is initialized with the input $u_0 = (u_{l_0}, u_{d_0}) = C(m^{des}, \xi_0)$ to the fourth cylinder during event 0 (initial event), where $\xi_0 = \xi^o$ is calculated based on the nominal engine data (Eq. 6). The first iteration of the controller algorithm (shown in Figure 8) starts with the feedforward controller calculating the control signals $u_i = (u_{l_i}, u_{d_i})$ during events $i = 1, 2, 3, 4$, that is,

$$u_i = C(m^{des}, \xi_{i-4}), \tag{23}$$

where, $\xi_l = \xi^o$ if $l \leq 0$. The conventional engine measurements ($\dot{m}_\phi$ and p_m) are used to compute the quantities y_1, y_2, y_3, and y_4 based on Eq. (12). For simplicity, we use here the equivalent compact state space representation (Eq. 13):

$$y_i = F_y\left(\chi_{[i\Delta,(i+1)\Delta]}\right). \tag{24}$$

Note that the inputs to cylinder 4 during the initialization and during the first cycle are kept constant, $u_0 = u_4$. This ensures the quasy-static periodic conditions in cylinder 4 for which the equalities $\hat{m}_0 = \hat{m}_4$, and $\mu_0^0 = \mu_4^4$ are satisfied, and we can obtain:

$$\begin{bmatrix} y_1 & y_2 & y_3 & y_4 \end{bmatrix}^T = \begin{bmatrix} 1-\mu_0^0 & \mu_1^1 & 0 & 0 \\ 0 & 1-\mu_1^1 & \mu_2^2 & 0 \\ 0 & 0 & 1-\mu_2^2 & \mu_3^3 \\ \mu_0^0 & 0 & 0 & 1-\mu_3^3 \end{bmatrix} \begin{bmatrix} \hat{m}_0 & \hat{m}_1 & \hat{m}_2 & \hat{m}_3 \end{bmatrix}^T. \tag{25}$$

In principle, we can now calculate the controller parameters (Eq. 10):

$$\begin{aligned} \xi_i &= \xi_{i-4} + \frac{\beta_i}{{\beta_i}^T\beta_i}\left(\hat{m}_i - {\beta_i}^T\xi_{i-4}\right) \\ &= K(u_i, \hat{m}_i, \xi_{i-4}),\ i = 0, 1, 2, 3. \end{aligned} \tag{26}$$

In the next iteration, however, only ξ_1 and ξ_2 are going to be used. Specifically, ξ_0 is not used because cylinder 4 has received already its inputs, u_4, and, moreover, y_4 has been sampled. In addition, ξ_3 is not updated but kept constant, $\xi_3 = \xi_{-1}$, in order to satisfy the periodic conditions for having $\hat{m}_3 = \hat{m}_7$, and $\mu_3^3 = \mu_7^7$ in the estimation algorithm. The feedforward controller parameters for the next iteration can, thus, be expressed as

$$\begin{bmatrix} \xi_0 \\ \xi_1 \\ \xi_2 \\ \xi_3 \end{bmatrix} = \begin{bmatrix} \xi^o \\ K(u_1, \hat{m}_1, \xi_{-3}) \\ K(u_2, \hat{m}_2, \xi_{-2}) \\ \xi_{-1} \end{bmatrix}. \tag{27}$$

The closed loop algorithm for the 4-cylinder engine is summarized. Consider $j = 0, 1, 2 \ldots$, then,

$$\begin{bmatrix} u_{3j+1} \\ u_{3j+2} \\ u_{3j+3} \\ u_{3j+4} \end{bmatrix} = \begin{bmatrix} C(m^{des}, \xi_{3j-3}) \\ C(m^{des}, \xi_{3j-2}) \\ C(m^{des}, \xi_{3j-1}) \\ C(m^{des}, \xi_{3j}) \end{bmatrix}, \tag{28}$$

$$\begin{bmatrix} y_{3j+1} \\ y_{3j+2} \\ y_{3j+3} \\ y_{3j+4} \end{bmatrix} = \begin{bmatrix} F_y\left(\chi_{[(3j+1)\Delta,(3j+2)\Delta]}\right) \\ F_y\left(\chi_{[(3j+2)\Delta,(3j+3)\Delta]}\right) \\ F_y\left(\chi_{[(3j+3)\Delta,(3j+4)\Delta]}\right) \\ F_y\left(\chi_{[(3j+4)\Delta,(3j+5)\Delta]}\right) \end{bmatrix}, \tag{29}$$

$$\begin{bmatrix} \hat{m}_{3j} & \hat{m}_{3j+1} & \hat{m}_{3j+2} & \hat{m}_{3j+3} \end{bmatrix}^T = \begin{bmatrix} 1-\mu_{3j}^{3j} & \mu_{3j+1}^{3j+1} & 0 & 0 \\ 0 & 1-\mu_{3j+1}^{3j+1} & \mu_{3j+2}^{3j+2} & 0 \\ 0 & 0 & 1-\mu_{3j+2}^{3j+2} & \mu_{3j+3}^{3j+3} \\ \mu_{3j}^{3j} & 0 & 0 & 1-\mu_{3j+3}^{3j+3} \end{bmatrix}^{-1} \times \begin{bmatrix} y_{3j+1} & y_{3j+2} & y_{3j+3} & y_{3j+4} \end{bmatrix}^T, \tag{30}$$

$$\begin{bmatrix} \xi_{3j} \\ \xi_{3j+1} \\ \xi_{3j+2} \\ \xi_{3j+3} \end{bmatrix} = \begin{bmatrix} \xi_{3j-4} \\ K(u_{3j+1}, \hat{m}_{3j+1}, \xi_{3j-3}) \\ K(u_{3j+2}, \hat{m}_{3j+2}, \xi_{3j-2}) \\ \xi_{3j-1} \end{bmatrix}, \tag{31}$$

with the initial condition

$$\begin{bmatrix} \xi_{-3} \\ \xi_{-2} \\ \xi_{-1} \\ \xi_0 \end{bmatrix} = \begin{bmatrix} \xi^o \\ \xi^o \\ \xi^o \\ \xi^o \end{bmatrix}. \tag{32}$$

Remark 1: In the closed loop controller algorithm, $n - (r-1)$ out of the n cylinders are adapted during an engine cycle.

Remark 2: The window of measurements (see Section 4 for the definition of the window of measurements) advances an engine cycle minus $(r-1)$ fundamental events each iteration of the controller algorithm. Thus, two consecutive windows of measurements have $(r-1)$ fundamental event overlap.

Remark 3: The first event after a change in desired cylinder air charge (m^{des}) and/or engine speed (N) the algorithm is initialized with the initial condition obtained from the previous step.

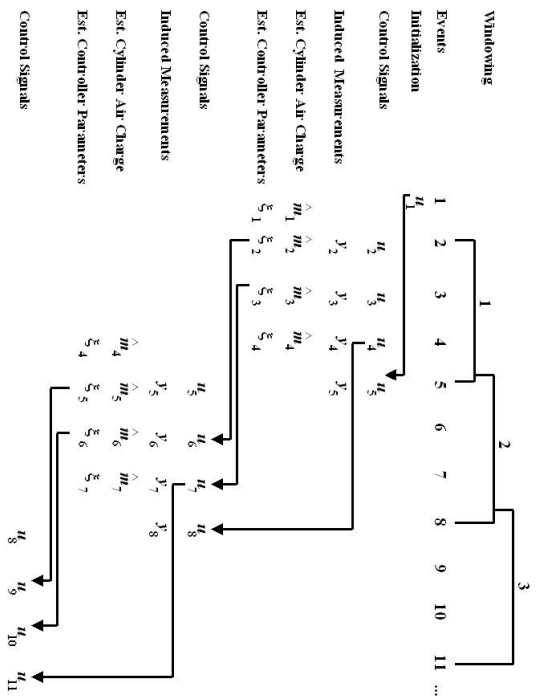

Figure 8: Flow chart of the closed loop controller algorithm for a 4-cylinder engine with 2-cylinder overlap ($r = 2$).

5.11. The General Case The closed loop controller algorithm for the n-cylinder engine with r-cylinder can be summarized as follows (see Figure 9 for the case of 3-cylinder overlap). Let the initial condition be

$$\begin{bmatrix} \xi_{-n+1} \\ \xi_{-n+2} \\ \vdots \\ \xi_0 \end{bmatrix} = \begin{bmatrix} \xi^o \\ \xi^o \\ \vdots \\ \xi^o \end{bmatrix}. \tag{33}$$

For $j = 0, 1, 2 \ldots$, we have:

$$\begin{bmatrix} u_{(n-(r-1))j+1} \\ u_{(n-(r-1))j+2} \\ \vdots \\ u_{(n-(r-1))j+n} \end{bmatrix} = \begin{bmatrix} C(m^{des}, \xi_{(n-(r-1))j-n+1}) \\ C(m^{des}, \xi_{(n-(r-1))j-n+2}) \\ \vdots \\ C(m^{des}, \xi_{(n-(r-1))j}) \end{bmatrix}, \tag{34}$$

$$\begin{bmatrix} y_{(n-(r-1))j+1} & y_{(n-(r-1))j+2} & \cdots & y_{(n-(r-1))j+n} \end{bmatrix}^T =$$

$$\begin{bmatrix} F_y\left(\chi_{[((n-(r-1))j+1)\Delta,((n-(r-1))j+2)\Delta]}\right) \\ F_y\left(\chi_{[((n-(r-1))j+2)\Delta,((n-(r-1))j+3)\Delta]}\right) \\ \vdots \\ F_y\left(\chi_{[((n-(r-1))j+n)\Delta,((n-(r-1))j+n+1)\Delta]}\right) \end{bmatrix}, \tag{35}$$

$$\begin{bmatrix} m_{(n-(r-1))j+1-(r-1)} \\ m_{(n-(r-1))j+2-(r-1)} \\ \vdots \\ m_{(n-(r-1))j+n-(r-1)} \end{bmatrix} = \tag{36}$$

$$\begin{bmatrix} \mu^{(n-(r-1))j+1-(r-1)}_{(n-(r-1))j+1} & \mu^{(n-(r-1))j+2-(r-1)}_{(n-(r-1))j+1} & \cdots & 0 \\ 0 & \mu^{(n-(r-1))j+2-(r-1)}_{(n-(r-1))j+2} & \cdots & 0 \\ \vdots & \vdots & \vdots & \vdots \\ \mu^{(n-(r-1))j+1-(r-1)}_{(n-(r-1))j} & \mu^{(n-(r-1))j+2-(r-1)}_{(n-(r-1))j} & \cdots & \mu^{nj+n-(r-1)}_{(n-(r-1))j+n} \end{bmatrix}^{-1}$$

$$\times \begin{bmatrix} y_{(n-(r-1))j+1} & y_{(n-(r-1))j+2} & \cdots & y_{(n-(r-1))j+n} \end{bmatrix}^T,$$

$$\begin{bmatrix} \xi_{(n-(r-1))j+1-(r-1)} \\ \vdots \\ \xi_{(n-(r-1))j} \\ \xi_{(n-(r-1))j+1} \\ \vdots \\ \xi_{(n-(r-1))j+n-2r} \\ \xi_{(n-(r-1))j+n-2r+1} \\ \vdots \\ \xi_{(n-(r-1))j+n-(r-1)} \end{bmatrix} = \tag{37}$$

$$\begin{bmatrix} \xi_{(n-(r-1))j+1-(r-1)} \\ \vdots \\ \xi_{(n-(r-1))j} \\ K(u_{(n-(r-1))j+1}, \hat{m}_{(n-(r-1))j+1}, \xi_{(n-(r-1))j+1-n}) \\ \vdots \\ K(u_{(n-(r-1))j+n-2r}, \hat{m}_{(n-(r-1))j+n-2r}, \xi_{(n-(r-1))j-2r}) \\ \xi_{(n-(r-1))j-2r+1} \\ \vdots \\ \xi_{(n-(r-1))j-(r-1)} \end{bmatrix},$$

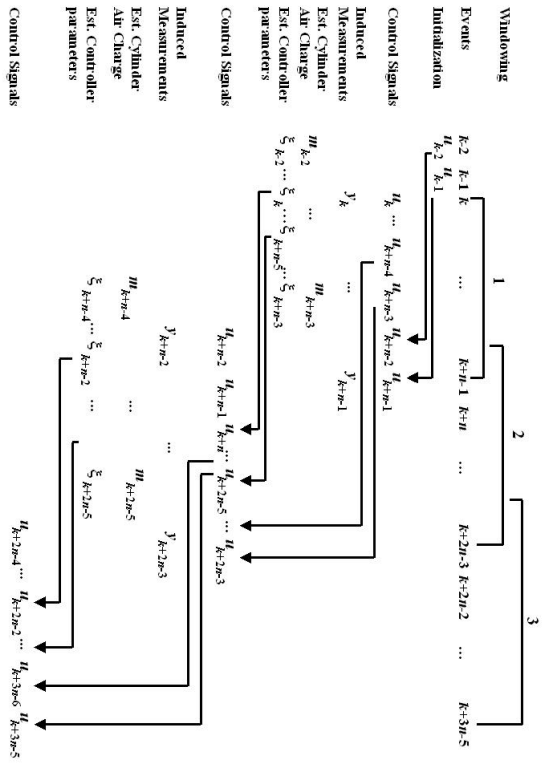

Figure 9: Flow chart of the closed loop controller algorithm for an n-cylinder engine with 3-cylinder overlap ($r = 3$).

6 Simulation Results

The simulations are chosen so that we test individually all of the components of the closed loop algorithm, specifically, the adaptive feedforward controller (Section 3) with the cylinder air charge estimation (Section 4). We gradually increase the requirements introducing model error and cylinder-to-cylinder overlap. Cycle-to-cycle tracking and cylinder-to-cylinder balancing is tested under different scenarios of engine and actuator conditions.

Figure 10 demonstrates the capabilities of the feedforward controller under nominal engine conditions. In this case, the controller is expected to track the desired cylinder air charge within one event (next firing cylinder if the communication and software implementation allow so) since no estimation and adaptation are needed. Indeed, it is shown that individual air charge follows the desired cylinder air charge (m^{des}) within one event. The simulation shows step changes in cylinder air charge, namely, from 0.35 g at $t = 0$ sec to 0.1 g at $t = 0.3$ sec, and finally, to 0.3 g at $t = 0.7$ sec. The demanded cylinder air charge is shown by the dotted line in Subplot 1, whereas, the actual cylinder air charge is plotted with the solid line and the markers (different marker for each cylinder). Note, that the distance between the markers corresponds to the intake event duration for each cylinder. In this Figure, the duration of the intake events is invariant because the simulation is performed at constant engine speed.

The control signals (u_d and u_l) are shown in Subplots 2 and 3. The control signals for the four cylinders are identical because the cylinders are balanced. The step changes in the demanded cylinder air charge forces the feedforward controller to switch between the branches of the "**L**" shape (see Section 3). In the first engine cycle ($t = [0, 0.08]$), the value of m^{des} is larger than the critical air charge (m_{cr}) and thus the feedforward controller selects $u_l = 7$ mm (subplot 2) and computes the corresponding $u_d = 134^o$ (subplot 3) that satisfies m^{des}. The small difference between the desired and individual cylinder air charge is due to errors in the curve fitting used in the feedforward controller. The closed loop controller algorithm balances the four cylinders within three engine cycles. The next value of m^{des} is less than m_{cr}. Thus, the feedforward controller selects $u_d = 80^o$ (subplot 3) and computes $u_l = 1.36$ mm (subplot 2) that satisfies m^{des}. As the desired cylinder air charge increases to 0.3 g, the individual air charge increases to a value less than m^{des}. The parameter estimator corrects for this error within two engine cycles.

The adaptive ability of the developed controller is tested during step changes in engine speed. The feedforward controller has been designed for 1500 RPM and step changes in engine speed alter the intake valve characteristics in a significant way (see Part I, Section 2.2). Thus, it is important to test the adaptive controller during rapid speed changes. To facilitate visualization, we fix the desired cylinder air charge, $m^{des} = 0.3$ g. The simulation results are shown in Figure 11. Engine speed (N) is varied twice. At $t = 0.45$ seconds, it decreases from 1500 RPM to 750 RPM and it increases to 3000 RPM for $t > 1.5$ seconds (Subplot 1). During the time interval $[0, 0.45]$ sec the controller corrects for curve fitting errors within two engine cycles. As the speed decreases to 750 RPM, the control signals (u_l and u_d) for the first five cylinders are initialized based on $N = 1500$ RPM conditions. The cylinder air charge is inversely proportional to engine speed for fixed intake valve lift and duration. Therefore, the individual cylinder air charge (Subplot 2) in the time interval $[0.45, 0.65]$ sec is larger than m^{des}. The controller parameter estimator predicts the variation and the error is corrected within two engine cycles. At $t = 1.5$ sec, the individual cylinder air charge of the following five cylinders drops below m^{des} due to the increase in engine speed. The controller then achieves air charge tracking within two engine cycles.

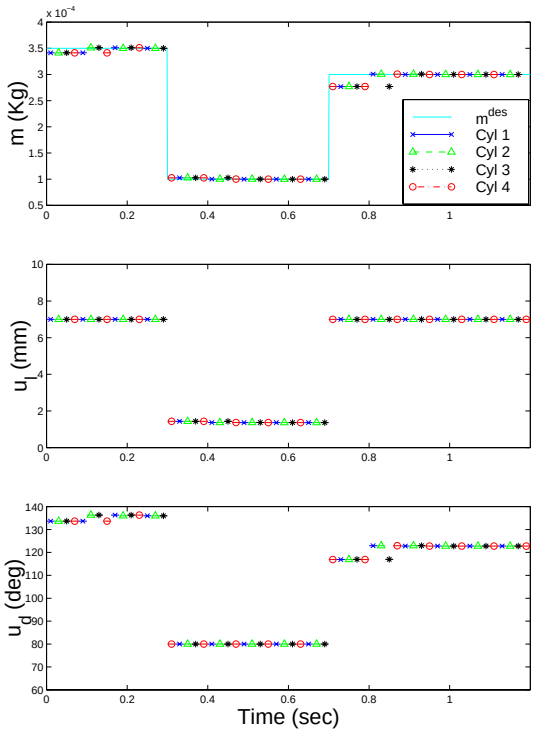

Figure 10: Nominal engine tracking.

The cylinder-to-cylinder balancing while tracking the cylinder air charge demand is demonstrated in Figure 12. In the simulation engine model we (i) reduce by 10% the valve effective area of cylinder 2 (represented by the marker "Δ") and (ii) introduce the Helmholtz resonator dynamics. The engine speed is equal to 6000 RPM which requires cylinder overlap during operation at medium-to-high loads. Indeed, during the first period $t < 0.1$ sec there is no cylinder overlap and the controller balances all the cylinders to the desired value. The step change in cylinder air charge to $m^{des} = 0.4$ g causes 2-cylinder

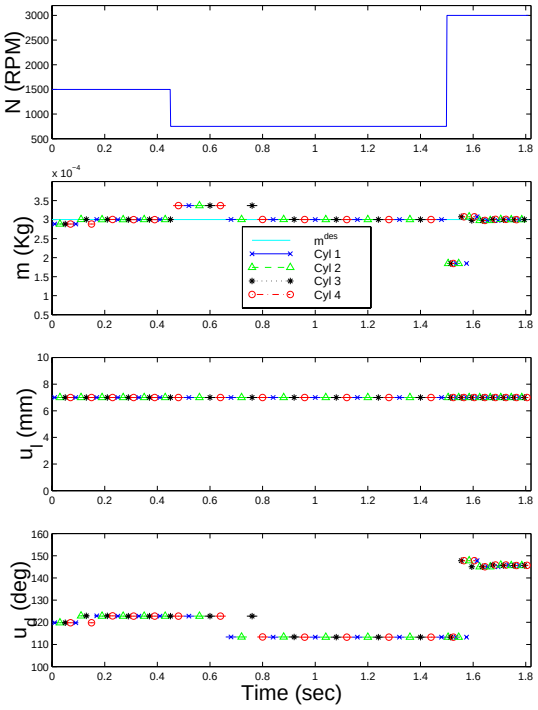

Figure 11: Air charge regulation during engine speed changes.

overlap. Thus, this simulation emulates

- significant cylinder-to-cylinder mixing,
- unknown model parameters, and
- unbalanced cylinders.

We compare the closed loop engine response (active adaptation algorithm) and the open loop response (we deactivate adaptation of the feedforward controller). In the first column of subplots we adapt the cylinders at all times. In the second column of subplots we trun off the adaptation algorithm when there is cylinder overlap ($t > 0.1$ seconds). The intended goal is to test the engine operation when we do not achieve accurate cylinder air charge estimation. For the comparison, let us define

$$E_{trk} \stackrel{\text{def}}{=} \max_j \mid m^{des} - m_j \mid \quad \text{tracking error, and} \tag{38}$$

$$E_{mld} \stackrel{\text{def}}{=} \max_{i,j} \mid m_i - m_j \mid \quad \text{maldistribution error} \tag{39}$$

where, $j = 1, \ldots, n$ for n number of cylinders. The tracking error refers to the maximum error between the desired air charge (or torque) and the individual cylinders. The maldistribution error refers to the maximum error between individual cylinders. Both have to converge to zero. The tracking error affects drivability. The maldistribution error affects drivability and can cause structural problems. The tracking error (E_{trk}) recorded in the case when the adaptation scheme is active is 1.5% which is small compared to the 10% change in valve area. Similar error (1.58%) was obtained for the case where the adaptation algorithm is turned off (top right subplot). The maldistribution error (E_{mld}), in the open loop case is, however, smaller, which indicates the benefits of deactivating the adaptation scheme during large modeling uncertainties and cylinder-overlap.

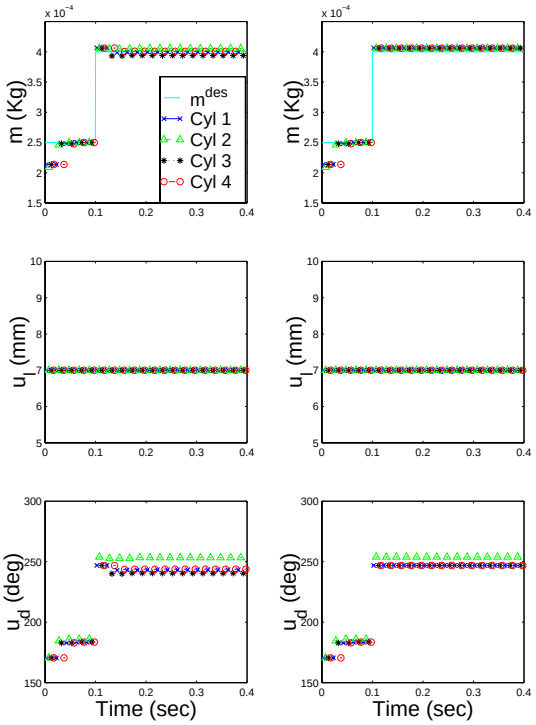

Figure 12: Cylinder balancing in the cylinder overlap case.

7 Acknowledgments

The authors would like to acknowledge helpful discussions with Jing Sun and Ilya Kolmanovsky of Ford Motor Co.

References

P. E. Moraal, J. A. Cook, and J. W. Grizzle, "Modeling the induction process of an automobile engine," *Control problems in industry,* I. Lasiecka and B. Morton, Ed., Birkhauser, pp. 253-270, 1995.

M. M. Schecter and M. B. Levin, "Camless Engine," SAE Paper No. 960581, 1996.

Ashhab M. S., Stefanopoulou A. G., Cook J. A., and Levin M., "Camless Engine Cotrol for Robust Unthrottled Operation," SAE Paper No. 981031.

K. Astrom and B. Wittenmark, Adaptive Control, Addison-Wesley Publishing Company, 1989.

H. Sono, H. Umiyams, "A Study of Combustion Stability of Non-throttling S. I. Engine with Early Intake Valve Closing Mechanism," SAE 945009.

O. Vogel, K. Rousssopoulos, L. Guzzella, and J. Czekai, "An Initial Study of Variable Valve Timing Implemented with a Secondary Valve in the Intake Runner," SAE Paper No. 960590, 1996.

Urata Y., Umiyama H., Shimizu K., Fujiyoshi Y., Sono H., and Fukuo K., "A Study of Vehicle Equipped with Non-Throttling SI Engine with Early Intake Valve Closing," SAE Paper No. 930820.